Non-invasive transdermal delivery of biomacromolecules with fluorocarbon-modified chitosan for melanoma immunotherapy and transdermal vaccines

Wenjun Zhu
Soochow University
Ting Wei
Soochow University
Qiutong Jin
Soochow University
Jiaqi Lu
Soochow University
Jun Xu
Soochow University
Muchao Chen
Soochow University
Jiafei Zhu
Soochow University
Yu Chao
Soochow University
Qian Chen
Soochow University
Zhuang Liu (zliu@suda.edu.cn)
Soochow University https://orcid.org/0000-0002-1629-1039

Article

Keywords: transdermal delivery, non-invasive, protein delivery, immunotherapy, SARS-CoV-2 vaccine

Posted Date: April 8th, 2022

DOI: https://doi.org/10.21203/rs.3.rs-1527855/v1

Abstract

Transdermal drug delivery has been regarded as an alternative to oral delivery and subcutaneous injection for its non-invasiveness, improved patient compliance and avoidance of the first-pass effect. However, needleless transdermal delivery of biomacromolecules remains a challenge. Herein, a transdermal delivery platform is developed to achieve highly efficient non-invasive transdermal delivery of biomacromolecules. In this system, fluorocarbon modified chitosan (FCS) is optimized as an effective yet biocompatible transdermal carrier to assemble with different proteins including immune checkpoint blockade (ICB) antibodies, and antigens such as the spike (S) protein of Severe Acute Respiratory Syndrome Coronavirus 2 (SARS-CoV-2). The formed FCS-containing nanocomplexes exhibited rather effective transdermal penetration ability via both intercellular and transappendageal routes. Interestingly, non-invasive transdermal delivery of ICB antibodies by FCS induced stronger immune responses to treat mouse melanoma compared to intravenous injection of free antibodies, while presenting reduced systemic toxicity. Moreover, transdermal delivery of SARS-CoV-2 vaccine using FCS-containing nanocomplexes resulted in comparable humoral immunity as well as improved cell immunity and immune memory compared to that achieved with subcutaneous vaccine injection. Thus, FCS-based transdermal delivery systems may provide a compelling opportunity to overcome the skin barrier for efficient transdermal delivery of biomacromolecules, widening the range of therapeutics that can be topically administered.

Introduction

Transdermal administration refers to needleless drug delivery across the skin without physical damages[1–3]. It has been regarded as an attractive alternative to oral delivery or subcutaneous injection of drugs, due to its unique advantages including non-invasiveness, avoidance of the first-pass effect, painless administration, better patient compliance, avoidance of needle phobia and so on[2,4,5]. Although a variety of transdermal enhancers have been proven to be effective in clinic, the delivered payloads are greatly limited to drugs which have molecular masses around a few hundred Daltons and exhibit strong hydrophobicity[6]. Nowadays, it is still difficult to realize efficient transdermal delivery of hydrophilic biomacromolecule such as peptides, proteins or nucleic acids[7]. Besides, the delivery of vaccines is currently one of the hottest research areas in both clinical and scientific communities considering the Coronavirus Disease 2019 (COVID-19) epidemic[8]. Compared to conventional subcutaneous injection or intramuscular injection, transdermal delivery of vaccines may be an attractive approach due to its possibility in at-home administration and the existence of the abundant immune cells in the skin[9].

To realize transdermal delivery of biomacromolecule drugs especially proteins, novel chemical enhancers such as membrane penetrating peptides, as well as various physical enhancement devices including cavitational ultrasound, electroporation, thermal ablation, microdermabrasion and microneedles have been developed[4,10–14]. Although such strategies could be used for transdermal delivery of various macromolecules including therapeutic proteins, they still face several concerns. For example, the

membrane penetrating peptides have been reported to enable transdermal delivery of small proteins such as insulin[15], but with unsatisfactory delivery efficiency[16], and remain to be ineffective for proteins with large molecular weights. Meanwhile, physical enhancement devices such as electroporation and sonophoresis not only can hardly be self-operated, but also could lead to skin damages by high energy pulses [17,18]. Microneedles, which refer to patches with many small needles, have been widely applied in transdermal delivery, showing great potential to delivery insulin and influenza vaccines in recent years[19]. However, the manufacturing process and quality control of microneedle patches especially with biomacromolecular payloads would be complicated. Additionally, the microneedles could still induce certain skin damages, which might increase the risk of infections. Therefore, it would be appealing to develop novel enhancers with high safety and efficiency for transdermal delivery of proteins.

Chitosan (CS) is a biodegradable natural cationic polymer with antibiotic activity and mucoadhesive property[20]. Inspired by the outstanding transmucosal efficiency of fluorocarbon modified CS (FCS) as reported in our previous study for intravesical-instillation-based bladder cancer treatment[21], we speculated that FCS may also be employed for transdermal delivery of biomacromolecules (Fig. 1a). Herein, we discovered that FCS could self-assemble with biomacromolecules such as proteins to form nanocomplexes, which could be added into Aquaphor® as a cream formulation for topical applications with greatly enhanced transdermal penetration ability. Using radiolabeled immunoglobulin G (IgG) as a model protein, we found that FCS/IgG-containing cream topically applied on the skin above a mouse melanoma could effectively deliver IgG into the tumor, and the peaked tumor uptake reached as high as 120 percent of injected dose per gram tissue (%ID/g).

We then employed such FCS-based transdermal delivery platform for tumor immunotherapy and SARS-CoV-2 vaccines. With the help of FCS, non-invasive transdermal delivery of anti-programmed death-ligand 1(aPDL1) antibody could effectively inhibit the growth of local tumors with direct contact to the FCS/aPDL1-containing cream. While combined with co-delivery of anti-cytotoxic T-lymphocyte-associated protein 4 (aCTLA4), such FCS/aPDL1/aCLTA4 cream could induce strong systemic immune responses to suppress both local and abscopal distant tumors, while showing reduced toxicity compared to intravenous injection of the two antibodies at the same dose. Furthermore, in a proof-of-concept experiment, we verified that FCS could form nanocomplexes with S1 protein of SARS-CoV-2 as the antigen, and polyinosinic : polycytidylic acid (PolyIC), a ligand for toll-like receptor (TLR) 3 as the adjuvant. Topical application of FCS/S1/polyIC nanocomplexes could trigger S1-protein-specific immune responses, reaching a level comparable to that achieved by subcutaneous injection of the same nanocomplex. Therefore, FCS developed in this work represents a rather effective carrier for transdermal delivery of biomacromolecules, offering exciting possibilities for a wide range of innovative applications such as localized melanoma immunotherapy and self-administrated transdermal vaccines against viruses (e.g. SARS-CoV-2).

Results And Discussion

Preparation of FCS/protein nanocomplexes and ex vivo evaluation of their transdermal abilities

FCS was synthesized following a previous report[22]. Briefly, perfluoroalkyl carboxylic acid (PFCA) was grafted to cationic polysaccharide CS through amide coupling at a fluorocarbon substitution of ~4.9% (**Figure S1**). Then, FCS was mixed proteins such as immunoglobulin G (IgG) and ovalbumin (OVA) at different mass ratios for 30 minutes under mild shaking to form nanocomplexes (**Figure 1a**). As shown in **Figure 1b & d**, both FCS/IgG and FCS/OVA with mass ratio at 1:1 showed sizes around 100 nm in the transmission electron microscopy (TEM) images, consistent with their hydrodynamic diameters measured by dynamic laser light scattering (DLS) (**Figure 1c & e**). The zeta potentials (ZP) of both FCS/IgG and FCS/OVA showed high positive charges, which increased from 6.97mV to 30.53mV and 4.38 mV to 36.73 mV, respectively, as the increase of FCS contents during the formation of nanocomplexes (**Figure 1e**). Then, the circular dichroism (CD) spectra were used to verify the structure of proteins before and after forming nanocomplexes. As shown in **Figure 1f**, FCS/IgG showed similar CD spectrum to that of free IgG, indicating that the structure of protein remained nearly unchanged during after formation of such FCS-containing nanocomplexes. Similar result also was found in the comparison between FCS/OVA and free OVA. Additionally, the antibody affinity of aPDL1 in the formulation of FCS/aPDL1 remained nearly unchanged as measured by the competition-enzyme-linked immunosorbent assay (ELISA) (**Figure S2**), further demonstrating that the formation of nanocomplexes wound not affect the activity of contained proteins.

Then, the transdermal kinetics and related mechanisms were investigated. Firstly, the standard Franz diffusion system was used to measure the transdermal delivery efficiency of FCS-containing nanocomplexes across the mouse skin layer. Briefly, fresh skin tissues were fixed between two glass cells, and then FCS/IgG or FCS/OVA, in which IgG and OVA were labelled with fluorescein (FITC), were added into the donor chamber. The transmitted IgG or OVA was measured by collecting liquid samples in the receptor chamber at different time points to measure the FITC fluorescence (**Figure 1g**). The transdermal delivery efficiencies of FCS/protein nanocomplexes with different feeding ratios (m/m) were measured. As shown in **Figure 1h**, FCS/IgG with the mass ratio at 1:1 showed the highest penetration ability across the skin, which may be contributed to the fact that FCS/IgG prepared at 1:1 showed the smallest sizes compared with those prepared at other mass ratio groups. It could be clearly observed that the zeta potentials of FCS/IgG nanocomplexes increased along with increasing the ratio of FCS, which may be beneficial for skin penetration. However, further increase of FCS might lead to the aggregation of nanocomplexes. On the other hand, when the amount of IgG increased, the zeta potential of FCS/IgG nanocomplex turned to be negative with aggregation, which is also unsuitable for skin penetration. Similarly, FCS/OVA with the mass ratio at 1:1 showed the highest penetration ability (**Figure 1i**). Therefore, all the data above confirmed the successfully transdermal delivery of FCS/protein nanocomplexes.

Transdermal mechanism of FCS-containing nanocomplexes

Next, we investigated the underlying transdermal mechanism of such FCS-containing nanocomplexes. According to previous literature, there are three classical permeation routes for transdermal delivery including intercellular, transappendageal and transcellular routes[23]. Firstly, we studied the intercellular route, by which the nanocomplexes could enlarge the space between epidermis cells and thus pass through them[24]. During the enlargement of intercellular space, we would expect the changes of cell resistance, as well as the expression and allocation of related proteins [25,26]. In this case, human skin dermis cells HACAT were used to form a cell monolayer and the transepithelial electrical resistance (TEER) between the two sides of monolayer was monitored (**Figure 2a**). As shown in **Figure 2b**, the cell single layer was formed 6 days later with stable and high TEER. Interestingly, an obvious decrease of TEER was observed with the addition of FCS/IgG on day 11, indicating the destruction of the cell monolayer and opening of intercellular channels after adding FCS-containing nanocomplexes. More interestingly, the re-increase of TEER was observed 4 hours later after the removal of FCS/IgG, and returned to its original level in 12 hours, demonstrating that FCS/IgG only temporarily opened the intercellular channel. TEM imaging of the skin also revealed the opening of the tight junctions and enlarged intercellular spaces after treatment with FCS/IgG compared with the normal skin (**Figure 2 & S4**). To confirm the enlargement of interstellar spaces, the changes of tight junctions (TJs) related protein such as zonula occludin (ZO)-1 were further evaluated[27]. With the addition of FCS/IgG, while the total expression of ZO-1 remained nearly unchanged, their continuous distribution was distinctly disturbed, indicating the opening of tight junctions along the interface between cells (**Figure 2c & 2d**). Moreover, the phosphorylation of myosin light chain, an important parameter for cytoskeletal structure[28], was found to be up-regulated in FCS/IgG treated cells, demonstrating that FCS was able to promote the phosphorylation of myosin light chain to induce the contraction of actin and the rearrangement of cytoskeleton (**Figure 2e**).

In addition to the enhanced intercellular bypass permeability of FCS-containing nanocomplexes, the transappendageal pathway, which usually plays an important role in the transport of large and water-soluble drugs through the hair follicles, sweat glands and sebaceous glands, was also investigated in our experiments [16]. With the counter-staining of Keratin (Krt) 14, the hair follicles and sweat glands in deep dermis region were labeled. As shown in **Figure 2g** (white arrows), it was observed that FCS/IgG colocalized with hair follicles and sweat glands, indicating that the tranappendageal pathway also played an important role in FCS-based transdermal delivery systems.

We further studied the transcellular route, which signifies the passage of drugs directly across keratinocytes[29]. Different from normal tissue cells which decompose drugs in lysosomes, polarized cells such as keratinocytes sometimes might expel drugs through exocytosis[24,30]. Apical exocytosis was used to investigate this phenomenon in vitro. Briefly, HACAT cells were incubated with FCS/IgG-FITC for endocytosis. After 12 h incubation, FCS/IgG-FITC were washed away and the cells were incubated for another 12 h. Then, the fluorescence of FITC in the supernatant was measured to evaluate the apical exocytosis. As shown in **Figure 2h**, the apical exocytosis rate of FCS/IgG-FITC from HACAT cells was less than 2%, almost the same compared with that treated with free IgG-FITC, indicating negligible

transcellular route was involved. Therefore, the transdermal delivery of FCS-containing nanocomplexes mainly relied on the intercellular and transappendageal pathways (**Figure 2i**).

Topical application of FCS/antibody nanocomplexes for melanoma treatment

Melanoma, one of the most common malignant tumors especially among Caucasians, poses an important threat to people's life and health[31]. For melanoma treatment, immunotherapy especially immune checkpoint blockade using anti-programmed death-1/its ligand (aPD1/aPDL1) antibodies has achieved excellent therapeutic efficacy in clinic[32]. Despite the exciting therapeutic result using aPD1/aPDL1 antibodies for the treatment of melanoma, there are still many limitations such as the risk of autoimmune diseases after intravenous injection[33]. Considering that FCS could act as the efficient transdermal delivery carrier for proteins, we thus used it as the transdermal delivery platform to deliver aPDL1 antibody for melanoma treatment (**Figure 3a**). It was expected that the transmitted aPDL1 could block the PD1/PDL1 pathway to stimulate cytotoxic T cells and lead to remarkable inhibition of tumors.

To examine the topical penetration behavior of antibodies complexed with FCS, tumors from the mice swiped with cream containing radioisotope ^{125}I labeled IgG (^{125}I-IgG) or FCS/^{125}I-IgG were collected for quantification of transmitted antibodies at different time points. As shown in **Figure 3b**, compared with free ^{125}I-IgG in the transdermally applied cream, FCS/^{125}I-IgG showed dramatically higher accumulation in tumor, while the radioactivities in other organs appeared to be much lower. Meanwhile, we found that the tumor accumulation of FCS/IgG showed the peaked level at over 120 % of injected dose per gram tissue (ID/g) at 12 h post the cream was applied (**Figure 3c**). As the cream was removed at 12 h, the IgG level in the tumor decreased slightly at 24 h. Meanwhile, the ELISA essay was also conducted to detect the tumor accumulation of IgG in the FCS/IgG formulation topically applied onto tumors in the cream. As shown in **Figure S5**, the ELISA essay showed similar results with the radiolabeling-based biodistribution data that IgG could be efficiently delivered into the tumor within 12 h with the aid of transdermal delivery platform using FCS/IgG nanocomplexes. On the other hand, the tumors with FCS/IgG-Cy5.5 were imbedded for tumor slicing. As illustrated in **Figure 3d**, the fluorescent signals of IgG-Cy5.5 in the tumor were gradually increased and evenly disbursed inside the whole tumor within 12 h, demonstrating the continuous transmission of antibodies from the FCS/IgG-Cy5.5 cream into the tumor.

Inspired by the effective accumulation of IgG in the tumor after transdermal delivery, we then carried out in vivo treatment for melanoma tumors by transdermal delivery of FCS/aPDL1. Mice bearing melanoma tumors were randomly divided into four groups: i. Untreated, ii. Free aPDL1 by intravenous (i.v.) injection, iii. CS/PDL1 in the cream by transdermal delivery and iv. FCS/aPDL1 in the cream by transdermal delivery. For transdermal delivery, CS/aPDL1 or FCS/aPDL1 solution was mixed with blank cream, and then applied on the tumor which was subsequently covered with a 3M® transparent film. Such treatment was repeated every two days for three times at the dose of 20 μg aPDL1 per mouse each time. For i.v. injection, 20 μg aPDL1 was administrated into each mouse every two days for three times. As another

control, aPDL1 was mixed with non-modified chitosan (CS/aPDL1) and added into the cream for topical application. As shown in **Figure 3e**, the tumors in FCS/aPDL1 treated group were successfully inhibited in a short time after the third treatment, while both CS/aPDL1 group and free aPDL1 group showed negligible anti-tumor efficacy. During 20 days of observation, the FCS/aPDL1 treated group exhibited the lowest tumor growth rate and the longest survival (**Figure S6**).

To understand the immune activation mechanisms of such transdermally delivered immunotherapy, tumors were collected from different groups on day 12 to investigate different types of immune cells especially T cells by flow cytometry. As shown in **Figure 3f**, for FCS/aPDL1 treated group, the percentages of both $CD4^+$ and $CD8^+$ T cells showed obvious increase in the tumor, indicating that aPDL1 was successfully delivered into the tumor to revert the T cell exhaustion. As Granzyme B is important for cell programming death triggered by $CD8^+$T cells, Ki67 is a cell proliferation, and Interferon γ is a cytokine associated with pro-apoptotic and antitumor mechanisms[34], we used these three markers to analyze the activities of CD8+ cells. As can be seen in **Figure 3g – 3i**, all of the three markers in $CD8^+$ T cells were increased in the FCS/aPDL1 group, suggesting the effective infiltration and activation of cytotoxic T lymphocytes (CTLs) in those tumors. For i.v. injection of aPDL1 and transdermal delivery of CS/aPDL1 groups, the tumor infiltrations of both $CD4^+$ and $CD8^+$ T cells as well as the expressions of granzyme B, Ki67 and IFN-g remained nearly unchanged, which might be resulted from the low tumor accumulation of aPDL1 after intravenous injection or transdermal delivery using CS. These results clearly indicated that, compared to i.v. injection of aPDL1, transdermal delivery aPDL1 using FCS resulted in enhanced antitumor immune responses.

Our platform could also be utilized to co-deliver different therapeutic proteins. In addition to aPDL1, anti-cytotoxic T-lymphocyte-associated protein 4 (aCTLA4) is another important antibody for immune checkpoint blockade to disable regulatory T cells (Tregs) and promote effective T-cell activation[35,36]. Thus, we further investigated the combination therapy using aPDL1 and aCTLA4 co-delivered by the transdermal delivery carrier FCS (**Figure 4a**). In this experiment, B16F10 cancer cells were inoculated on the right flank of each mouse as the primary tumor, and a second tumor was inoculated on the opposite site of the same mouse to mimic the cancer metastasis. Three days later, mice bearing two melanoma tumors were randomly divided into five groups: i. Untreated, ii. Free aPDL1 and aCTLA4 (i.v.), iii. FCS/aPDL1, iv. FCS/aCTLA4, v. FCS/aPDL1/aCTLA4. All the groups were administrated for three times with 20 μg aPDL1 and 20 μg aCTLA4 per mouse each time. It is worth pointing out that after the second i.v. injection of aPDL1 + aCTLA4, half of mice in this group died, likely due to the horrible side effects (e.g. cytokine storm) triggered by systemic administration of both aPDL1 and aCTLA4. In contrast, the other groups with transdermal delivery of immune checkpoint blockade antibodies showed negligible abnormality. Excitingly, compared to FCS/aPDL1 or FCS/aCTLA4 treated mice, noteworthy synergistic therapeutic effect was achieved by combination therapy with transdermally delivered FCS/aPDL1/aCTLA4 (**Figure 4b & 4c**). More interestingly, the growth of distant tumors in mice with FCS/aPDL1/aCTLA4 treatment also was inhibited (**Figure 4d & 4e**). To understand the abscopal effect induced by FCS/aPDL1/aCTLA4, the distant tumors were collected 12 days after different treatments and

analyzed by flow cytometry. Consistent with the above results, the number of $CD8^+$ T cells especially $Ki67^+CD8^+$ T cells exhibited obvious increase in the second tumor (**Figure 4f & 4i**), and the percentages of Tregs were decreased in FCS/aPDL1/aCTLA4 treated group (**Figure 4j**).

The excellent anti-tumor efficacy and the increased CTLs in the distant tumor might be attributed to the following mechanisms. Firstly, the activation of CTLs in the local tumor could induce immunogenic death of tumor cells and trigger the chronic exposure of damage-associated molecular patterns (DAMPs) as well as tumor antigens. Antigen presenting cells (APCs) are then activated and subsequently present tumor antigens to $CD8^+$ T cells, further amplifying systemic antitumor immunity to attack distant tumors. Lastly, as reported, the blockade of PDL1 in the tumor-draining lymph nodes (TDLNs), which may be more efficient to be reached by transdermal delivery, could effectively propel systemic anti-tumor T cell immunity even in distant tumor sites[37,38]. Therefore, our transdermal immune checkpoint antibody delivery could achieve remarkable antitumor efficacies against both in local and distant tumors.

Topical application of FCS/S1/polyIC nanocomplexes for transdermal vaccination

Vaccine is another area of great interest for transdermal delivery[39]. For transdermal vaccine, in addition to avoiding syringe by health professionals, it could improve immune responses by targeting abundant immune cells beneath the epidermis layer. Since the outbreak of Coronavirus Disease 2019 (COVID-19), various vaccines have been developed to suppress the infection of SARS-CoV-2[40–42]. Up to now, more than 180 SARS-CoV-2 vaccines are under research worldwide, and 26 SARS-CoV-2 vaccines are in the stage of clinical trials[43]. However, all these vaccines need subcutaneous or intramuscular injection, which not only require well-trained medical staffs, but also face some additional issues such as disposal of a large number of sterile syringes. The transdermal SARS-CoV-2 vaccine, on the other hand, may offer great assistance to prevent COVID-19 by self-administration, especially in areas with tight medical resources. Considering the rapid global spread of COVID-19, and the efficient transdermal delivery of antibody using FCS, we further explored whether FCS could be utilized to transdermally deliver SARS-CoV-2 vaccine in a proof-of-concept study.

To synthesize FCS-based subunit SARS-CoV-2 vaccine, FCS were mixed with the S1 subunit of spike protein of SARS-CoV-2 virus and polyIC, forming the transdermal SARS-CoV-2 vaccine (FCS/S1/polyIC) (**Figure 5a**). Note that poly IC as a double-strand RNA is a toll-like receptor 3 (TLR 3) agonist that has been commonly used as immune adjuvant[44]. We also optimized the ratio of FCS : antigen : PolyIC in the FCS/S1/PolyIC vaccine. In this experiment, OVA was used as a modulate antigen for the optimization of formulation. As shown in **Figure 5c & d**, FCS/OVA/polyIC with different mass ratio showed variant sizes at about 200 nm and increased zeta potential with the increase of FCS. For the skin penetration ability measured by Franz diffusion system in **Figure 5e**, FCS/OVA/PolyIC prepared at the mass ratio at 2:1:1 with relatively small sizes showed the highest skin permeability, and thus this formulation was used for further study.

For the in vivo vaccination experiments, mice were randomly divided into three groups: i. untreated, ii. transdermal delivery of FCS/S1/polyIC, and iii. subcutaneous (s.c.) injection of S1/polyIC. As shown in **Figure 5b**, mice in transdermal delivery group were administrated 3 times in 2 weeks (the doses of S1 and polyIC were both 20 μg per time), while mice in s.c. injection group were injected twice with the S1 protein dose at 20 μg per time and the polyIC dose at 50 μg per time. Interestingly, mice with transdermal delivery of FCS/S1/polyIC showed almost similar antibody titer to that of mice with s.c. injection of S1/polyIC in two weeks, indicating that the transdermal delivery of FCS/S1/PolyIC could result in almost the same B cell activation level compared with s.c. administrated vaccines (**Figure 5f**). Furthermore, after boosting on day 14, the specific antibody titers in both transdermal delivery group and s.c. injection group reached up to 10^4 in 30 days, further indicating the effective activation of humoral immunity by those vaccines. After another boost on day 42, mice vaccinated by either transdermal delivery of FCS/S1/polyIC or s.c. injection of S1/polyIC showed remained at high levels of anti-S1 antibody titers.

In addition to the activation of humoral immunity by generating specific antibody against the S1 protein, the cell immunity also plays an important role in virus clearance by training cytotoxic T cells to recognize and kill virus-infected host cells [45–47]. Therefore, the levels of cytotoxic T cells in mouse spleen were evaluated on day 28 after the primeval administration. Although no obvious change of $CD4^+$ and $CD8^+$ T cell infiltration was observed in different groups (**Figure 5g & 5h**), the secretion of IFN-g by $CD4^+$ T cells and $CD8^+$ T cell was obviously increased in mice after transdermal delivery of FCS/S1/PolyIC compared to that in mice by s.c. injection of S1/polyIC (**Figure 5i & 5j**), indicating that stronger cytotoxic T cell responses was induced by transdermal delivery of S1 vaccine. Moreover, the percentage of both memory $CD4^+$ and $CD8^+$ T cells in the spleen of mice treated with FCS/S1/polyIC was also dramatically increased on day 90 (**Figure S14**), while those in mice with subcutaneous administration of S1/PolyIC appeared to be much lower, demonstrating that the transdermal delivery of vaccines would trigger long-term adaptive immune memory effect, which might be resulted from the long retention of co-delivered antigen and adjuvant.

In order to investigate the exact permeation ability of vaccines after transdermal administration, we measured the accumulation of antigens in the lymph node 24 h post transdermal delivery or subcutaneous injection of vaccine using Cy5.5-labeled OVA as the modal antigen. As expected, compared to s.c. injection of OVA, mice after transdermal delivery of vaccine after completely swiping the cream off the skin surface showed lower OVA retention according to the IVIS imaging system (**Figure S15**). Then we further evaluated the uptake of OVA by DCs in lymph nodes and skin (**Figure 5k & 5l**). Interestingly, even though the percentage of OVA^+ DCs in lymph node of mice with s.c. injection was higher than that of mice with transdermal delivery, the DCs beneath skins showed higher OVA uptake in mice treated by the cream containing FCS/OVA/polyIC, revealing that the transdermal delivery of vaccine could directly activate DCs in situ and the activated DCs could migrate to lymph nodes to trigger further immune responses. In contrast, for the s.c. injection group, antigen and adjuvant would migrate to lymph nodes separately, and were more likely to be depleted by non-specific immune cells and activate DCs with low effectiveness[48].

Additionally, we measured the maturation of DC and the activation of $CD8^+$ T cell on one and three days after different treatments. As shown in Figure **5m & 5n**, the mice with transdermal delivery of vaccines showed almost similar DC maturation and T cell activation to that of mice with s.c. injection, consistent with the observed T cell activation in the spleen. Therefore, although FCS-based transdermal delivery of vaccine showed less absolute antigen penetration compared to that with s.c. injection, it could trigger almost similar humoral immunity and stronger cell immunity. The additional advantages of such FCS-based transdermal vaccines would be the possibility in self-administration and preferable user compliance. However, further studies such as SARS-CoV-2 virus challenge was not conducted due to our current limitations of experimental conditions in handling viruses.

Conclusion

In conclusion, we developed a transdermal delivery system based on FCS for efficient local delivery of biomacromolecules including antibodies, antigens, or nucleic acids (e.g. polyIC), which could be mixed with FCS and added into a cream for topical applications. For transdermal delivery of antibodies such as aPDL1 and aCTLA4, our FCS-based delivery systems could result in high local antibody accumulation in melanomas and rather strong T cell responses, and thus successfully eliminated primary tumors and inhibited the growth of distant tumors on mice. With significantly enhanced therapeutic responses compared to systemic injection of antibodies at the same dose, our FCS-based local delivery of immune checkpoint antibodies may lead to less concerns in systemic side effects considering the relatively low serum concentrations by the topical administration route. On the other hand, transdermal delivery of SARS-CoV-2 vaccines resulted in S1-specific antibody titer similar to that achieved by s.c. injection, and even stronger T cell responses. Such transdermal delivery of SARS-CoV-2 vaccines might enable fast and vast vaccination even at home once this strategy was proven to be effective in further studies. Our work thus realized effective noninvasive needleless transdermal delivery of macromolecular therapeutics without the need of any additional physical or chemical stimulations, which has been rather challenging via existing techniques. In addition to delivering immune checkpoint antibodies and vaccines, the macromolecular transdermal delivery carrier developed in this work may also be employed for transdermal delivery of other therapeutic biomacromolecules aiming at diverse medical applications, and holds tremendous potential for commercialization.

Declarations

Acknowledgement

This article was partially supported by the National Research Programs of China (No. 2021YFF0701800, 2020YFA0211100), the National Natural Science Foundation of China (Nos. 52032008, 91959104, 21927803, 51903182), the Natural Science Foundation of Jiangsu Province (No. BK20190826), Emergency Research Project of COVID-19 from Zhejiang University, Collaborative Innovation Center of Suzhou Nano Science and Technology, and the 111 Program from the Ministry of Education of China.

References

1. Prausnitz, M. R. & Langer, R. Transdermal drug delivery. Nat. Biotechnol. **26**, 1261–1268 (2008).
2. Prausnitz, M. R., Mitragotri, S. & Langer, R. Current status and future potential of transdermal drug delivery. Nat. Rev. Drug Discov. **3**, 115–124 (2004).
3. Alkilani, A., McCrudden, M. T. & Donnelly, R. Transdermal Drug Delivery: Innovative Pharmaceutical Developments Based on Disruption of the Barrier Properties of the Stratum Corneum. Pharmaceutics **7**, 438–470 (2015).
4. Prausnitz, M. R. Microneedles for transdermal drug delivery. Adv. Drug Deliv. Rev. **56**, 581–587 (2004).
5. Naik, A., Kalia, Y. N. & Guy, R. H. Transdermal drug delivery: overcoming the skin's barrier function. Pharm. Sci. Technolo. Today **3**, 318–326 (2000).
6. Karande, P., Jain, A., Ergun, K., Kispersky, V. & Mitragotri, S. Design principles of chemical penetration enhancers for transdermal drug delivery. *Proc. Natl. Acad. Sci.* **102**, 4688–4693 (2005).
7. Amjadi, M., Mostaghaci, B. & Sitti, M. Recent Advances in Skin Penetration Enhancers for Transdermal Gene and Drug Delivery. Curr. Gene Ther. **17**, (2017).
8. Ahn, D.-G. *et al.* Current Status of Epidemiology, Diagnosis, Therapeutics, and Vaccines for Novel Coronavirus Disease 2019 (COVID-19). J. Microbiol. Biotechnol. **30**, 313–324 (2020).
9. Ita, K. Transdermal delivery of vaccines – Recent progress and critical issues. Biomed. Pharmacother. **83**, 1080–1088 (2016).
10. Lee, P. J., Ahmad, N., Langer, R., Mitragotri, S. & Prasad Shastri, V. Evaluation of chemical enhancers in the transdermal delivery of lidocaine. Int. J. Pharm. **308**, 33–39 (2006).
11. Mutalik, S., Parekh, H. S., Davies, N. M. & Nayanabhirama, U. A combined approach of chemical enhancers and sonophoresis for the transdermal delivery of tizanidine hydrochloride. Drug Deliv. **16**, 82–91 (2009).
12. Murthy, S. N. & Hiremath, S. R. R. Physical and chemical permeation enhancers in transdermal delivery of terbutaline sulphate. AAPS PharmSciTech **2**, 1–5 (2001).
13. Nasrollahi, S. A., Taghibiglou, C., Azizi, E. & Farboud, E. S. Cell-penetrating Peptides as a Novel Transdermal Drug Delivery System. Chem. Biol. Drug Des. **80**, 639–646 (2012).
14. Desai, P., Patlolla, R. R. & Singh, M. Interaction of nanoparticles and cell-penetrating peptides with skin for transdermal drug delivery. Mol. Membr. Biol. **27**, 247–259 (2010).
15. Chen, Y. *et al.* Transdermal protein delivery by a coadministered peptide identified via phage display. Nat. Biotechnol. **24**, 455–460 (2006).
16. Marwah, H., Garg, T., Goyal, A. K. & Rath, G. Permeation enhancer strategies in transdermal drug delivery. Drug Deliv. **23**, 564–578 (2016).
17. Cross, S. & Roberts, M. Physical Enhancement of Transdermal Drug Application: Is Delivery Technology Keeping up with Pharmaceutical Development? Curr. Drug Deliv. **1**, 81–92 (2004).

18. Nanda, A., Nanda, S. & Khan Ghilzai, N. Current Developments Using Emerging Transdermal Technologies In Physical Enhancement Methods. Curr. Drug Deliv. **3**, 233–242 (2006).
19. Tran, K. T. M. *et al.* Transdermal microneedles for the programmable burst release of multiple vaccine payloads. Nat. Biomed. Eng. (2020). doi:10.1038/s41551-020-00650-4
20. Shariatinia, Z. Pharmaceutical applications of chitosan. Adv. Colloid Interface Sci. **263**, 131–194 (2019).
21. Cheng, Y. Design of polymers for intracellular protein and peptide delivery. Chinese J. Chem. cjoc.202000655 (2021). doi:10.1002/cjoc.202000655
22. Li, G. *et al.* Fluorinated Chitosan To Enhance Transmucosal Delivery of Sonosensitizer-Conjugated Catalase for Sonodynamic Bladder Cancer Treatment Post-intravesical Instillation. ACS Nano **14**, 1586–1599 (2020).
23. Zhou, X. *et al.* Nano-formulations for transdermal drug delivery: A review. Chinese Chem. Lett. **29**, 1713–1724 (2018).
24. Niu, X.-Q. *et al.* Mechanism investigation of ethosomes transdermal permeation. Int. J. Pharm. X **1**, 100027 (2019).
25. Antonescu, I. E. *et al.* The Permeation of Acamprosate Is Predominantly Caused by Paracellular Diffusion across Caco-2 Cell Monolayers: A Paracellular Modeling Approach. Mol. Pharm. **16**, 4636–4650 (2019).
26. Bittermann, K. & Goss, K.-U. Predicting apparent passive permeability of Caco-2 and MDCK cell-monolayers: A mechanistic model. PLoS One **12**, e0190319 (2017).
27. Ahmadi, S. *et al.* A human-origin probiotic cocktail ameliorates aging-related leaky gut and inflammation via modulating the microbiota/taurine/tight junction axis. JCI Insight **5**, (2020).
28. Robert-Paganin, J., Pylypenko, O., Kikuti, C., Sweeney, H. L. & Houdusse, A. Force Generation by Myosin Motors: A Structural Perspective. Chem. Rev. **120**, 5–35 (2020).
29. Kováčik, A., Kopečná, M. & Vávrová, K. Permeation enhancers in transdermal drug delivery: benefits and limitations. Expert Opin. Drug Deliv. **17**, 145–155 (2020).
30. Fan, K. *et al.* Ferritin Nanocarrier Traverses the Blood Brain Barrier and Kills Glioma. ACS Nano **12**, 4105–4115 (2018).
31. Miller, A. J. & Mihm, M. C. Melanoma. N. Engl. J. Med. **355**, 51–65 (2006).
32. Franklin, C., Livingstone, E., Roesch, A., Schilling, B. & Schadendorf, D. Immunotherapy in melanoma: Recent advances and future directions. Eur. J. Surg. Oncol. **43**, 604–611 (2017).
33. Martin-Liberal, J., Kordbacheh, T. & Larkin, J. Safety of pembrolizumab for the treatment of melanoma. Expert Opin. Drug Saf. **14**, 957–964 (2015).
34. Cao, X. *et al.* Granzyme B and Perforin Are Important for Regulatory T Cell-Mediated Suppression of Tumor Clearance. Immunity **27**, 635–646 (2007).
35. Wei, S. C. *et al.* Distinct Cellular Mechanisms Underlie Anti-CTLA-4 and Anti-PD-1 Checkpoint Blockade. Cell **170**, 1120–1133.e17 (2017).

36. Seidel, J. A., Otsuka, A. & Kabashima, K. Anti-PD-1 and Anti-CTLA-4 Therapies in Cancer: Mechanisms of Action, Efficacy, and Limitations. Front. Oncol. **8**, (2018).
37. Dammeijer, F. *et al.* The PD-1/PD-L1-Checkpoint Restrains T cell Immunity in Tumor-Draining Lymph Nodes. Cancer Cell **38**, 685–700.e8 (2020).
38. Jiang, W. *et al.* Exhausted CD8 + T Cells in the Tumor Immune Microenvironment: New Pathways to Therapy. Front. Immunol. **11**, (2021).
39. Pielenhofer, J., Sohl, J., Windbergs, M., Langguth, P. & Radsak, M. P. Current Progress in Particle-Based Systems for Transdermal Vaccine Delivery. Front. Immunol. **11**, (2020).
40. Corbett, K. S. *et al.* SARS-CoV-2 mRNA vaccine design enabled by prototype pathogen preparedness. Nature **586**, 567–571 (2020).
41. Elia, U. *et al.* Design of SARS-CoV-2 hFc-Conjugated Receptor-Binding Domain mRNA Vaccine Delivered via Lipid Nanoparticles. ACS Nano acsnano.0c10180 (2021). doi:10.1021/acsnano.0c10180
42. Zhang, N.-N. *et al.* A Thermostable mRNA Vaccine against COVID-19. Cell **182**, 1271–1283.e16 (2020).
43. Krammer, F. SARS-CoV-2 vaccines in development. Nature **586**, 516–527 (2020).
44. Cheng, Y. & Xu, F. Anticancer function of polyinosinic-polycytidylic acid. Cancer Biol. Ther. **10**, 1219–1223 (2010).
45. Rydyznski Moderbacher, C. *et al.* Antigen-Specific Adaptive Immunity to SARS-CoV-2 in Acute COVID-19 and Associations with Age and Disease Severity. Cell **183**, 996–1012.e19 (2020).
46. Shi, J., Li, Y., Chang, W., Zhang, X. & Wang, F.-S. Current progress in host innate and adaptive immunity against hepatitis C virus infection. Hepatol. Int. **11**, 374–383 (2017).
47. Rahe, M. & Murtaugh, M. Mechanisms of Adaptive Immunity to Porcine Reproductive and Respiratory Syndrome Virus. Viruses **9**, 148 (2017).
48. Schudel, A., Francis, D. M. & Thomas, S. N. Material design for lymph node drug delivery. Nat. Rev. Mater. **4**, 415–428 (2019).

Figures

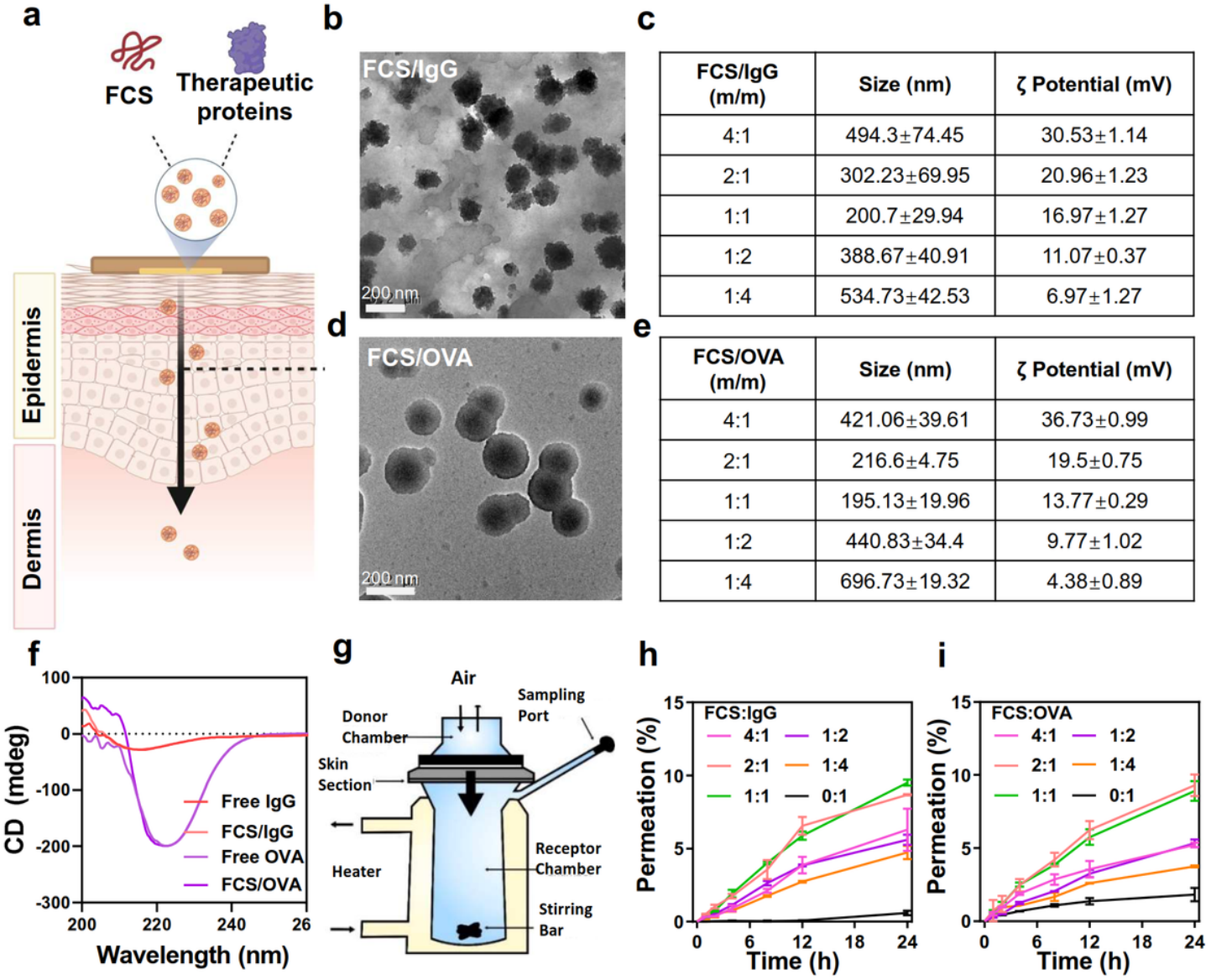

FCS/IgG (m/m)	Size (nm)	ζ Potential (mV)
4:1	494.3±74.45	30.53±1.14
2:1	302.23±69.95	20.96±1.23
1:1	200.7±29.94	16.97±1.27
1:2	388.67±40.91	11.07±0.37
1:4	534.73±42.53	6.97±1.27

FCS/OVA (m/m)	Size (nm)	ζ Potential (mV)
4:1	421.06±39.61	36.73±0.99
2:1	216.6±4.75	19.5±0.75
1:1	195.13±19.96	13.77±0.29
1:2	440.83±34.4	9.77±1.02
1:4	696.73±19.32	4.38±0.89

Figure 1

The characterization of FCS-containing nanocomplexes. (a) The schematic image of FCS-containing nanocomplexes for transdermal delivery. (b) Representative TEM images of FCS/IgG and (d) FCS/OVA. (c&e) Size distribution and zeta potential of FCS-containing nanocomplexes including (c) FCS/IgG and (e) FCS/OVA. (f) Circular Dichroism (CD) spectra of proteins pre and post FCS coating. (g) Schematic illustration of Franz diffusion cell system used for the skin permeation study. (h) Cumulative percentage of FCS/IgG-FITC and (i) FCS/OVA-FITC permeated across the skin after incubation with different FCS-containing formulations over time. All illustrations were created with BioRender.com. Data are presented as mean ± standard deviation (n=3).

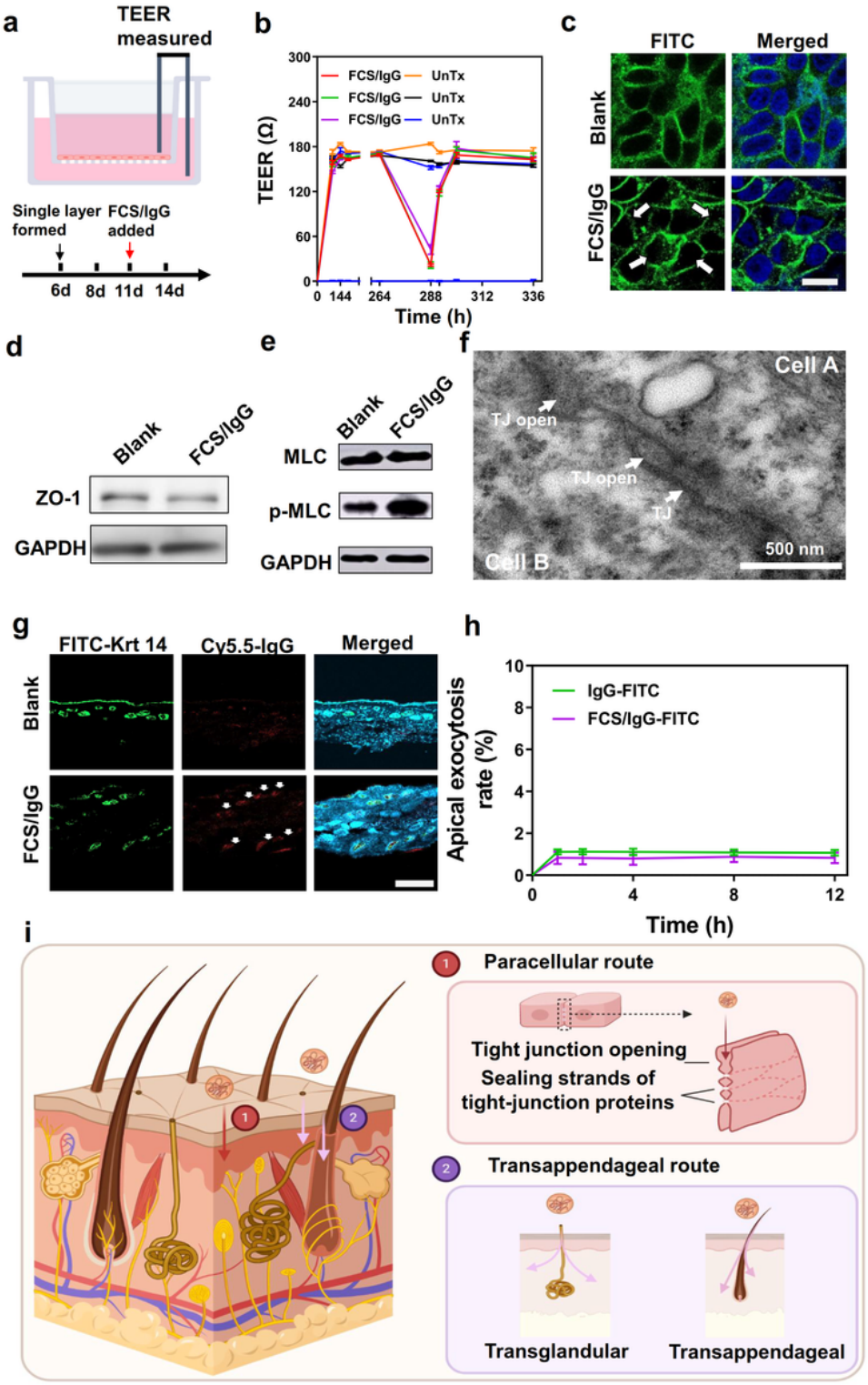

Figure 2

The transdermal mechanism of FCS-containing nanocomplexes. (a) Illustration of HACAT monolayer cell model. (b) Effects of FCS/IgG on the TEER of the HACAT monolayer cell model. (c) Immunofluorescence images of the distribution of tight junction related protein ZO-1 on the HACAT cell membrane after being treated with FCS/IgG. The white arrows indicated the allocation change of ZO-1. (d&e) Western blotting images showing ZO-1 and the phosphorylated level of MLC in cells after incubation with FCS/IgG. (f)

Representative TEM image of skin epithelium after being treated with FCS/IgG. The white arrows indicated the tight junctions (TJs) and the opening of TJs. (g) Representative immunofluorescence images exhibiting the colocalization of keratin 14 and FCS/IgG-Cy5.5 (white arrows). (h) The apical exocytosis rate of HACAT cells after being incubated with different FCS formulations for 12 hours. (i) The schematic image of the transdermal mechanisms. FCS-containing nanocomplexes could penetrate skin epidermis through both paracellular and transappendageal routes. By the paracellular route, FCS could stimulate the phosphorylation of MLC and thus open the tight junction between epidermis cells by sealing strands of tight junction proteins. By the transappendageal route, FCS-containing nanocomplexes could cross the epidermis through hair follicles and sweat glands. All illustrations were created with BioRender.com. Data are presented as mean ± standard deviation (n=3).

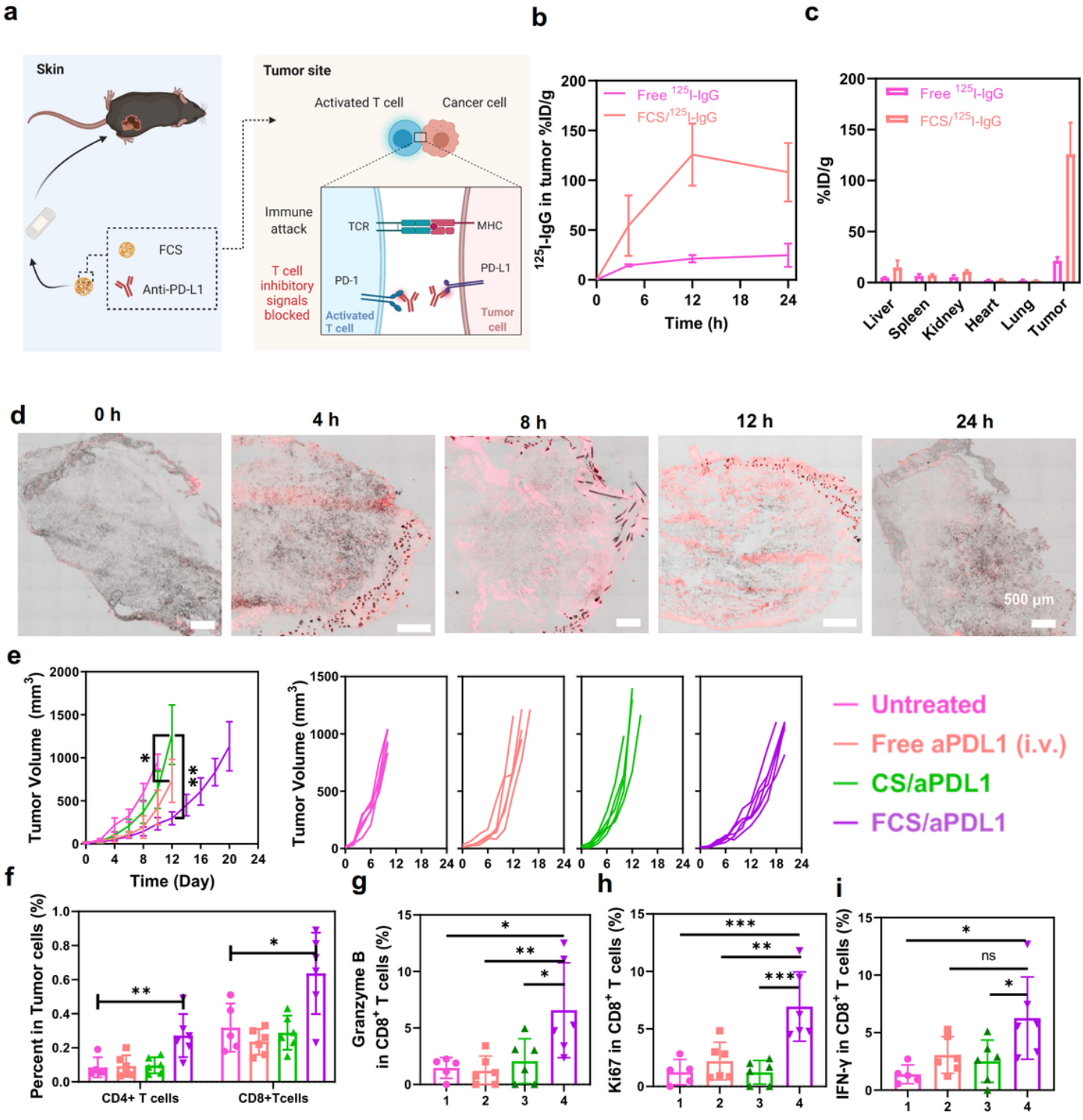

Figure 3

Transdermal delivery of aPDL1 for the treatment of B16F10 melanoma tumors. (a) Schematic illusions illustrating the localized transdermal administration of FCS/aPDL1&FCS/aCTLA4 for the treatment of B16F10 melanoma tumors. (b) The accumulation of FCS/^{125}I-IgG in the tumor at different time intervals. (c) Biodistribution of FCS/^{125}I-IgG at 12 h based on radioactivity measurement. (d) Representative confocal images showing the accumulation of FCS/IgG-Cy5.5 in the tumor at different time intervals.

Scale bar: 500 μm. (e) Tumor growth curves of mice in different groups. Growth curves were stopped when the first mouse in the related group was dead or its tumor size exceeded 1,000 mm^3. (f) Quantification of $CD4^+$ T cells and $CD8^+$ T cells in the tumor after different treatments. The representative flow cytometric plots were illustrated in **Figure S7**. (g-i) Quantification of granzyme B^+ ($CD3^+CD8^+$Granzyme B^+), $Ki67^+$ ($CD3^+CD8^+Ki67^+$) and IFN-γ^+ ($CD3^+CD8^+$ IFN-γ^+) T cells in the tumor after different treatments. The representative flow cytometric plots were illustrated in **Figure S8-S10**. All illustrations were created with BioRender.com. Data are presented as mean ± standard deviation (n=6). Statistical significance was calculated via one-way ANOVA with a Tukey post-hoc test. *P < 0.05; **P < 0.01; ***P < 0.001.

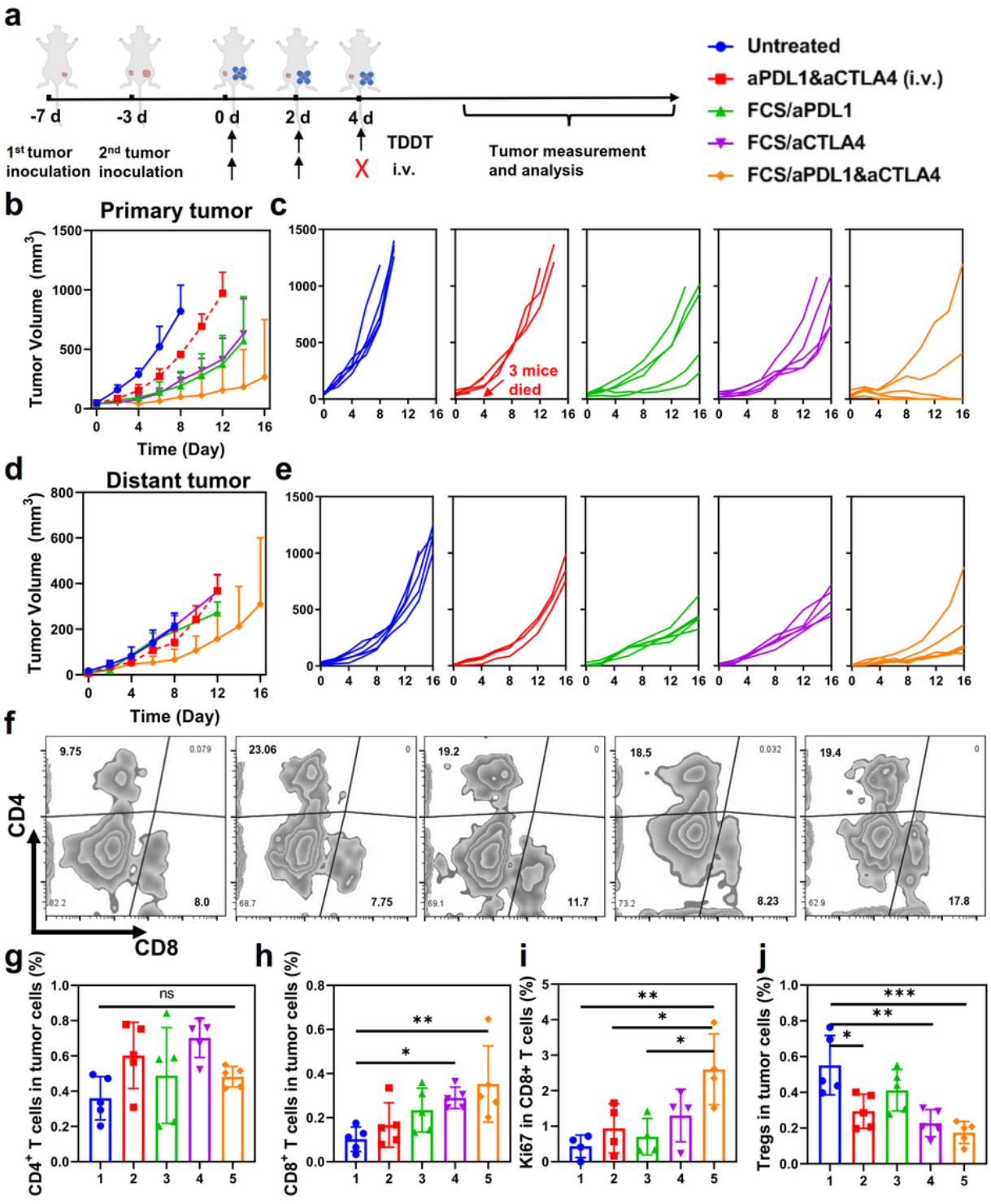

Figure 4

The abscopal effect induced by transdermal delivery of combined immune checkpoint antibodies. (a) Schematic illustration of transdermal co-delivery of aPDL1 and aCTLA4 to inhibit the growth of both primary and distant tumors. (b-e) Tumor growth curves of primary and distant tumors after different treatments. Growth curves were stopped when the first mouse in the related group was dead or the first mouse's tumor size exceeded 1,000 mm^3. (f-h) Representative flow cytometry plots (f) and the related

quantification of (g) $CD4^+$ T cells and (h) $CD8^+$ T cells in distant tumors after different treatments. (i&j) Quantification of $Ki67^+$ ($CD3^+CD8^+Ki67^+$) T cells (i) and Tregs ($CD3^+CD4^+Foxp3^+$) (j) in distant tumors after different treatments. The representative flow cytometric plots were illustrated in **Figure S11.** Data are presented as mean ± standard deviation (n=5). Statistical significance was calculated via one-way ANOVA with a Tukey post-hoc test. *P < 0.05; **P < 0.01; ***P < 0.001.

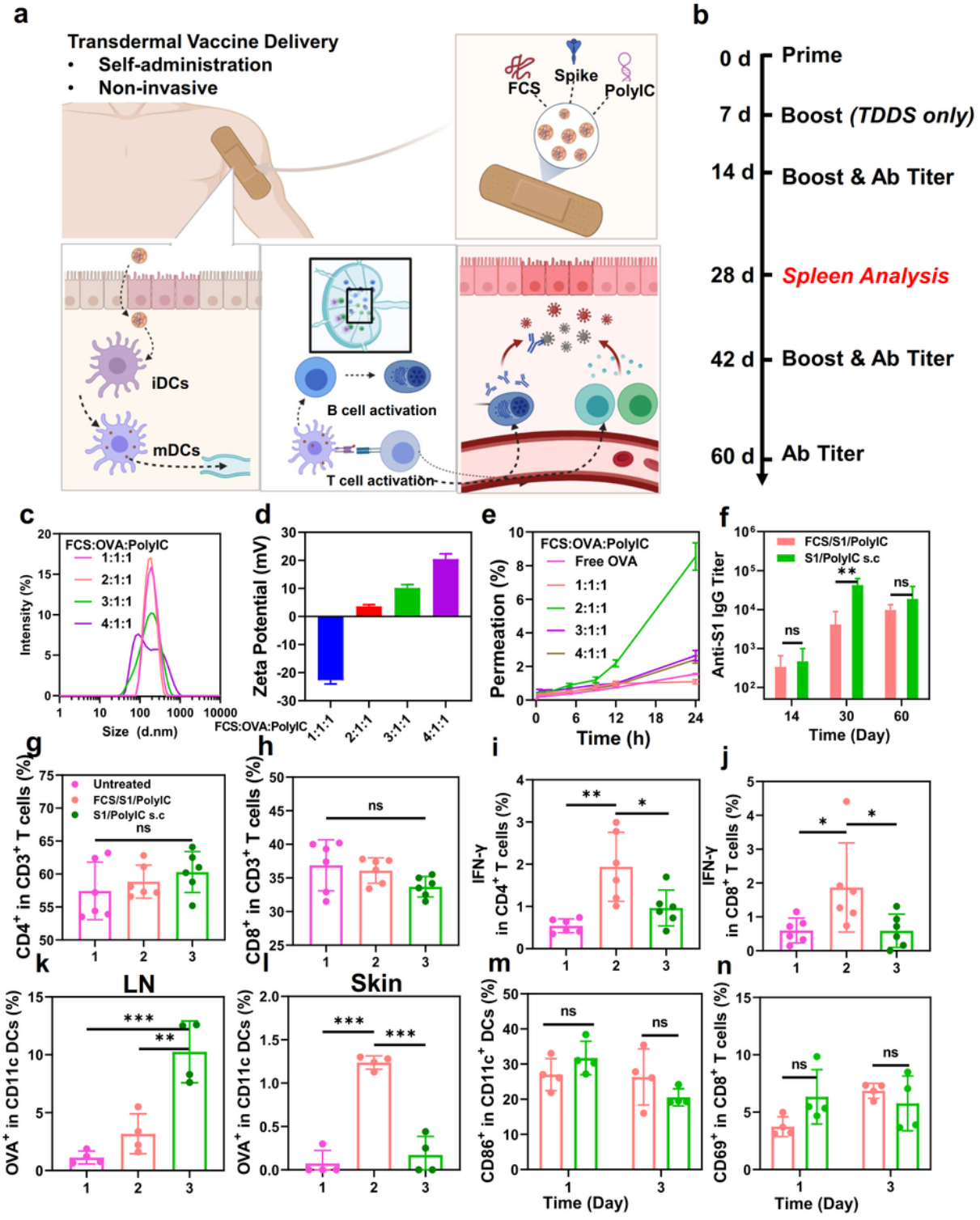

Figure 5

Transdermal delivery of SARS-CoV-2 vaccine. (a) A schematic illustration for transdermal delivery of SARS-CoV-2 vaccine and the triggered immune responses. After transdermal delivery, such SARS-CoV-2 nano-vaccines could activate immune cells such as DCs in the dermis, or migrate to the nearby lymph nodes for immune activation. (b) Schematic illustration of the experimental design showing transdermal delivery of SARS-CoV-2 vaccine. (c&d) DLS (c) and zeta potential (d) of FCS-based transdermal vaccines with different mass ratios from 1:1:1 to 4:1:1. (e) The skin penetration ability of FCS-based transdermal vaccine with different mass ratios. (f) SARS-CoV-2 specific IgG antibody titers at different time intervals determined by ELISA. (g&h) Quantification of $CD4^+$ T cells, $CD8^+$ T cells in the spleen at day 28. (i&j) Quantification of IFN-γ^+ secreting $CD4^+$ T cells ($CD3^+CD4^+$ IFN-γ^+) and $CD8^+$ T cells ($CD3^+CD8^+$ IFN-γ^+) in the spleen at day 28. (k&l) Quantification of OVA-$Cy5.5^+$ ($CD45^+CD11c^+Cy5.5^+$) in DCs in (k) lymph nodes and (l) skin. (m&n) Quantification of (m) DC maturation ($CD45^+CD11c^+CD86^+$) and (n) T cell receptor (TCR) activation ($CD45^+CD3^+CD8^+CD69^+$) in lymph nodes. All illustrations were created with BioRender.com. The representative flow cytometric plots were illustrated in **Figure S12 & S13.** Data are presented as mean ± standard deviation (n=4 or 6). Statistical significance was calculated via one-way ANOVA with a Tukey post-hoc test. *P < 0.05; **P < 0.01; ***P < 0.001.

Supplementary Files

This is a list of supplementary files associated with this preprint. Click to download.

- SI20220405NBT.docx